Comparison of Three Hybrid Turbulence Models for the Flow Around a 25 ◦ Ahmed Body

F. Delassaux, V. Herbert, I. Mortazavi, C. Ribes

Comparison of three hybrid turbulence models for the flow around a 25°Ahmed body

F. Delassaux, V. Herbert, I. Mortazavi & C. Ribes

Abstract The flow around the 25°Ahmed body has been studied computationally by applying different methods including an improved URANS formulation, the SAS model and two popular hybrid RANS/LES formulations: DDES and SBES models. All of the turbulence models employ the underlying SST RANS formulation. These hybrid models show a good prediction for the drag coefficient, with an error between 0 and 4% compared to experiments, whereas the discrepancy is slightly more important for the lift coefficient. The DDES model shows the best representation of the flow features between all the models studied.

1 Introduction

The automotive industry is facing drastic restrictions regarding greenhouse gas emissions, with the objective of 95 g/km of CO_2 emission from 2020. To reach this goal, reducing fuel consumption from aerodynamics drag is one of the main issues for engineers. Bluff body flows are characterized by regions of separated flows containing wide spectra of turbulent scales. These regions are mainly responsible for drag and lift forces applied on the body. Turbulence modelling must be capable of giving a fair prediction of separation to accurately predict the global flow features. Hence, the purpose of this work is to fine-tune a robust Scale Resolving Simulations (SRS) procedure on the 25° Ahmed body before moving on to real vehicles.

The 25°Ahmed body is a very complex case with strong longitudinal vortices which interacts with the recirculation bubble on the rear slant surface and the 3D

Francois Delassaux - Iraj Mortazavi
Equipe M2N, CNAM Paris, 292 rue Saint-Martin, 75003 Paris
e-mail: francois.delassaux@ext.mpsa.com

Vincent Herbert - Charles Ribes
Groupe PSA, Route de Gisy, 78943 Velizy-Villacoublay

wake structure. Steady state or transient RANS simulations have shown huge difficulties to predict correctly the flow around 25°Ahmed body [4], [6]. Besides, Large Eddy Simulation (LES) model shows interesting results from different studies [8], [13]. However, the prohibitive numerical cost of LES is not feasible for industrial flow for the next future. Hence, a SRS approach is needed to represent the wide scales and spectrum of turbulence for such cases. Three different approaches are used: an improved URANS formulation, the SAS [11] and hybrid RANS-LES models, DDES [15] and SBES [2], detailed in Sect. 3. The DES97 approach [14] was used by Kapadia et al. [7] using Spalart-Allmaras underlying RANS model. The authors faced Modeled-Stress Depletion (MSD) because of LES intrusion in the boundary layer, as the mesh is not fine enough to handle LES resolution in the boundary layer. As a consequence, the flow separates massively on the rear slant surface. Menter and Kuntz [10] observed a fully stalled flow on the rear window with SST RANS model. Using SST DES, a closed recirculation bubble was observed, even though the time-averaged solution did not closely match with experiments. The coarse grid used in this study could explain the results discrepancy from experiments. Guilmineau et al. [5] used SST DES with both $F_{DES} = 0$, F_1 and F_2 shielding functions to switch from RANS to LES resolutions. Both $F_{DES} = 0$ and F_1 functions capture the separation/attachment phenomenon on the rear slant surface, even though the bubble recirculation length was overestimated. As the F_2 function over-protects the boundary layer, a massive separation flow is predicted. More recently, Ashton et al. [3] demonstrated the accuracy of the DDES models using both SST and $\phi - f$ underlying RANS models.

In first instance, the main purpose of this work is to explore new hybrid turbulence models and evaluate their predictive capabilities on simplified geometry car. The paper is organized as follows: Sect. 2 describes the Ahmed body used in the numerical study. Sect. 3 provides some details on the turbulence modelling approaches. Then, Sect. 4 enumerates both the numerical setup and the grid. Sect. 5 shows the influence of the grid refinement around the rear surface on the flow topology. Finally, Sect. 6 compares CFD results and experiments on 25°Ahmed body.

2 Ahmed body geometry

The Ahmed body [1] is a simplified real car, made of a forebody, a long mid-section assumed to suppress interactions between the front and the back of the body and a variable rear slant angle. The length, width, and height of the body are respectively $L_B = 1044$ mm, $W_B = 380$ mm and $H_B = 288$ mm. The angle φ between horizontal line and the rear slant surface is equal to 25°. The body is fixed to the wind tunnel ground with four feet, defined by a diameter of 30 mm and a ground clearance of $G = 50$ mm. The stilts are used in this study in order to make more complex the underbody flow stream, as can be found on real car. The origin of the (x,y,z) axis is located at the vertical base of the body, on the ground, see Fig. 1. Besides, the

projected length of the rear slant surface is defined as $L = 201$ mm and used for dimensionless plots.

Our numerical results are compared to Rossitto [13] experiments, made in La Ferté Vidame (France) wind tunnel.

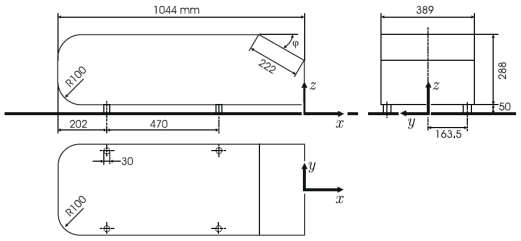

Fig. 1 Properties of the 25° Ahmed body geometry

3 Turbulence models

This study compares three different turbulence modeling approaches: an improved RANS formulation, the Scale-Adaptive Simulation (SAS), and hybrid RANS-LES formulations, Delayed Detached Eddy Simulation (DDES) and Stress-Blended Eddy Simulation (SBES) using ANSYS Fluent software. For both models, RANS underlying model is the SST k-ω developed by Menter [9], known as the more accurate turbulence model for separation prediction compared to $k-\varepsilon$ and $k-\omega$ formulations.

3.1 Scale-Adaptive Simulation - SAS

SAS is an improved URANS formulation developed by Menter and Egorov [11] based on Rotta's work. This approach allows the representation of the large scales of turbulence, which is not the case with traditional $k-\varepsilon$ and $k-\omega$ RANS models. The authors modify and adapt the Rotta's model to the $k-\omega$ SST approach, defining the SST SAS model. The only difference between RANS and SAS formulations is the additional source term denoted Q_{SAS} in the transport equation for ω:

$$Q_{SAS} = max\left[\rho\eta_2\kappa S^2\left(\frac{L}{L_{vk}}\right)^2 - C\cdot\frac{2\rho k}{\sigma_\phi}max\left(\frac{1}{\omega^2}\frac{\partial\omega}{\partial x_j}\frac{\partial\omega}{\partial x_j},\frac{1}{k^2}\frac{\partial k}{\partial x_j}\frac{\partial k}{\partial x_j}\right),0\right] \quad (1)$$

Where ρ, κ, S^2, L, L_{vk}, k and ω are respectively the density, the von Kármán constant, the strain rate magnitude, the length scale of the modeled turbulence, the von Kármán length scale, the turbulent kinetic energy and the turbulent eddy frequency. η_2, C and σ_ϕ are constant parameters. The von Kármán length scale is defined as follow:

$$L_{vk} = \kappa \left| \frac{U'}{U''} \right| \tag{2}$$

With $U' = \sqrt{2S_{ij}S_{ij}}$ and $S_{ij} = \frac{1}{2}\left(\frac{\partial U_i}{\partial x_j} + \frac{\partial U_j}{\partial x_i}\right)$. The second derivative of L_{vk} term (see Eq.2) detects instabilities in the flow, and then allows the break-up of large unsteady structure into a turbulent spectrum. This is possible by the reduction of the eddy viscosity, allowing flow fluctuations. The source term Q_{SAS} dominates the other terms of the ω equation, under unsteady conditions, then activated the full SAS functionality, acting like LES subgrid model.

3.2 Delayed Detached Eddy Simulation - DDES

The DDES is a hybrid RANS-LES formulation developed by Spalart et al. [15], and is an improvement of the original formulation DES97 [14]. The main feature of the DES model is to compute flow using RANS formulation in attached boundary layers zone and switch to LES resolution away from the wall, when separation occurs. The model length scale is then modified and the switch is done by a shielding function designed to protect the boundary layer from the LES intrusion. For DDES model, the shielding function takes into account both the distance to the wall and eddy-viscosity field, which is time-dependent. The shielding function f_d is defined as follow by Spalart et al. [15]:

$$f_d = 1 - tanh\left[(C_{d1} r_d)^{C_{d2}}\right] \tag{3}$$

The r_d parameter, defined in [15], represents the ratio of a model length scale to the wall distance. The f_d function is designed to be equal to 1 in LES region, where $r \ll 1$, and 0 elsewhere with $r_d > 1$. The constants C_{d1} and C_{d2} are respectively 20 and 3 to ensure a fair protection of boundary layer with SST model. The DDES length scale reads as follow:

$$l_{DDES} = l_{RANS} - f_d \, max(0, l_{RANS} - l_{LES}) \tag{4}$$

With $l_{RANS} = \frac{\sqrt{k}}{\beta^* \omega}$, $l_{LES} = C_{DES}.\Delta_{max}$, Δ_{max} the maximum local grid spacing $\Delta_{max} = max(\Delta_x, \Delta_y, \Delta_z)$ and $C_{DES} = C_{DES}^{k-\omega}.F_1 + C_{DES}^{k-\varepsilon}.(1 - F_1)$ with $C_{DES}^{k-\omega} = 0.78$ and $C_{DES}^{k-\varepsilon} = 0.61$. The $F1$ function defines the location of the blending between the $k-\omega$ and $k-\varepsilon$ models in the boundary layer [9].

3.3 Stress-Blended Eddy Simulation - SBES

SBES is a new hybrid RANS-LES turbulence model with a modified formulation, compared to DDES, giving the ability to switch from underlying RANS model directly to any existing algebraic LES model [2]. The LES resolution is made by the Wall-Adapting Local Eddy-viscosity (WALE) model. The SBES shielding function is the same as the one developed in Shielded Detached Eddy Simulation model (SDES) [2], called f_{SDES}. This function theoretically enhances the shielding function compared to DDES by a better protection of the RANS wall boundary layer region against influences from the LES mode. This function has not been published yet. The shielding function f_{SDES} achieves the blending on the stress level between RANS and LES formulations as follow:

$$\tau_{ij}^{SBES} = f_{SDES}\tau_{ij}^{RANS} + (1 - f_{SDES})\,\tau_{ij}^{LES} \tag{5}$$

The same formulation is done for the blending of eddy viscosity. This new formulation represents a new type of hybrid RANS-LES approach with the ability to choose both RANS and LES models.

4 Numerical setup and grid

The computational domain is respectively $5L_B$ long upstream and $10L_B$ long downstream of the Ahmed body. The cross section of domain is equal to $4.2L_B$ and its height is set to $5L_B$, giving a blockage ratio of $0,5\%$. The inlet boundary condition is defined as velocity inlet with $V_\infty = 40\ m/s$. A pressure outlet condition is applied to the exit surface, with gauge pressure equal to 0 Pa. No-slip wall boundary conditions have been applied on the body based on the integration of the governing equations down to the wall itself. The same boundary conditions are used on the sides of the computational domain as the blockage ratio is low. The ground of the computational domain is divided into two parts: from the inlet to $X/L_B = 3$, a slip wall condition is applied. For the remainder part of the ground, a no-slip wall condition is used to allow the build up of the boundary layer. The demarcation between these two parts allows to reproduce the experimental boundary layer thickness [13].

For the boundary layers resolution around the body and the ground domain, 30 prism layers are used starting from 0.007 mm to 16 mm with the stretch factor of 1.232. The whole domain is fitted by tetrahedron cells with box refinement in strategic locations of the flow (forebody, underbody and rear slant surface) to capture the separation/attachment phenomenon, as shown with the red line in Fig. 2. The grid contains 22 million cells. The wall normal resolution is $y+ < 0.7$. In the streamwise and spanwise directions, the mesh is refined as $30 < \Delta s^+ = \Delta l^+ < 250$ for the rear slant, with a mean value of $\Delta s^+ = \Delta l^+ \approx 120$. Besides, the time step is fixed as $\Delta t = 5.10^{-5}$ s, leading to a non-dimensionnal time step $\Delta t.V_\infty/L_B = 0.002$. This time step ensures a CFL number around 1 in critical areas of the flow. The com-

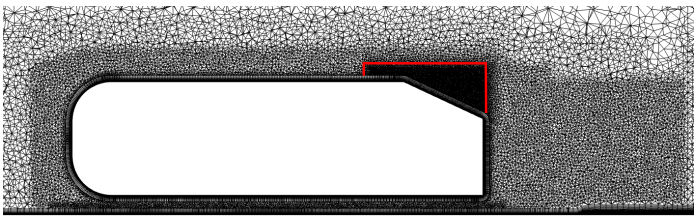

Fig. 2 Mesh in symmetry plane Y0 - the red curve shows the position of the box refinement around the rear surface

putations were run for a total of 115 convective transit times defined as $T.V_\infty/L_B$, with $T = 3$ seconds of physical time. The time-averaging process was started after 77 transit times, to be sure of the relevance of the averaged quantities.

5 Focus on refinement box

The grid convergence study has shown that DDES model is more accurate but more sensitive to grid refinement compared to SAS and SBES. A focus was made on the transition between prisms and tetrahedrons cells around the rear slant, in the location shown by the red line in Fig. 2. Two different parameters have been studied to observe their influence on the final solution. The first parameter is the growth rate (GR) of the tetrahedron cells expansion. The second one is the reference length (L_{ref}) of the tetrahedron cells. The L_{ref} coefficient is used to determine the maximum cell volume, based on a perfect volume tetrahedron cell and defined as: $V = (L_{ref}^3\sqrt{2})/12$. In order to capture the shear layer emanating from the detachment of the flow on the backlight, the setup used for the Reference mesh, described in Sect. 4, is as follow: $GR = 1.15$ and $L_{ref} = 3$ mm.

The Tab. 1 summarizes both the values of GR, L_{ref} and drag and lift coefficient differences on four grids for DDES only. The grids called “Reference” and “2”, described in Tab. 1, show globally the same results on the aerodynamics coefficients, meaning that the global flow topology is fairly reproduced (separation/attachment on the rear slant surface and fair prediction of the position of longitudinal vortices), as described in Sect. 6. Grids “1” and “3”, with very low Cd and Cl coefficients compared to experiments, clearly indicate a massive separation of the flow on the backlight, as for the 35° configuration. For the DDES model, the reference length L_{ref} of the tetrahedron cells is the most important parameter to reproduce the expexted flow topology of the 25° Ahmed body. It shows the grid-dependence of the DDES method compared to SAS or SBES, that expressed closer results for the four grids studied. However, the best DDES result is closer to experiments than the two other techniques.

Table 1 Comparisons of drag and lift coefficients between experiments and DDES on different grids

Grids	GR	$L_{ref}[mm]$	Number of cells [M]	$\Delta Cd[\%]$	$\Delta Cl[\%]$
Reference	1.15	3	22	0.1	6.3
1	1.15	10	18.5	-26.4	-120.5
2	1.37	3	21.4	0.7	6.9
3	1.37	10	18.2	-26.7	-121.5

Table 2 Comparisons of drag and lift coefficients between experiments, SAS, DDES and SBES models

Models	C_d	$\Delta C_d\,[\%]$	C_l	$\Delta C_l\,[\%]$
Experiments	0.356	-	0.311	-
SAS	0.355	- 0.3	0.298	- 4.0
DDES	0.356	0.1	0.331	6.3
SBES	0.341	- 4.2	0.328	5.4

6 Numerical results

In this section, three turbulence models are compared to wind tunnel experiments [13] based on the Reference grid described in Sect. 4 and Sect. 5. The CFD methodology is validated below and the flow behaviour is studied on the 25° Ahmed body.

The drag and lift coefficients are compared to experiments results in Tab. 2. Both turbulence modeling correctly predict the drag coefficient, with no prediction error for SAS and DDES and a 4% error for SBES. SAS is the best prediction regarding drag and lift coefficients. This result must be put in perspective as the SAS flow topology is less representative of the experimental flow, compared to DDES and SBES. Also, it seems that error compensation all along the body give a close Cl coefficient with experiments. On the contrary, DDES and SBES that clearly predict a closed separation bubble on the rear slant surface show respectively 6.3% and 5.4% errors on Cl. These errors are mainly due to the three surfaces responsible for lift force: the rear slant surface, the roof and the underbody.

One of the main feature of the flow around the 25° Ahmed body is the closed recirculation bubble on the rear slant surface. The bubble recirculation length L_R, defined as the ratio between the recirculation bubble length over the rear slant surface length, is equal to 78% in experiments. The Tab. 3 below compares the zero-velocity contours on the back part of the body. The DDES model shows the best prediction for the recirculation bubble length, equal to 90%. SBES leads to a smaller closed recirculation, with L_R equal to 53%. On the contrary, SAS shows a reattachment at the end of the rear slant surface, so that L_R is equal to 100 %.

Table 3 Zero velocity $\overline{U_x}$ contours for SAS, DDES and SBES models - $L_R = 78\%$ in experiments

SAS	DDES	SBES
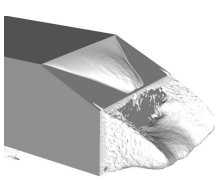	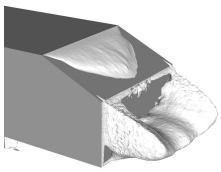	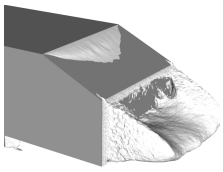
$L_R = 100\%$	$L_R = 90\%$	$L_R = 53\%$

The Fig. 3 compares the mean streamwise velocity $\overline{U_x}$ and the mean total turbulent kinetic energy $\overline{TKE}$ profiles between turbulence models and experiments, in the symmetry plane $Y/L = 0$. Here, the recirculation zone is represented by the evolution of the velocity and TKE correlated profiles, with positive and negative velocity values that reflect the recirculating flow direction. The best prediction of the flow with DDES is clearly observable on the velocity profiles. Due to the close reattachment zone between experiments and DDES, a very good agreement is obtained on the rear slant surface and in the wake of the body in the symmetry plane. The quick reattachment of the SBES model is clear, as the formation of a boundary layer is observable at the location $x/L = -0.5$. On the contrary, the SAS reattachment zone is only situated at the end of the rear slant surface, so that low velocity is notable at all locations of velocity measurement (in the recirculation region). However, due to the different flow topologies on the rear window, some discrepancies appear on the upper part of the body wake.
The peak of $\overline{TKE}$ emanating from the shear layer separation, on the top of the rear slant angle is slightly under-estimated in the first three measurement locations (from $x/L = -0.9$ to $x/L = -0.7$) for DDES and SAS models. Consequently, the length of the recirculation bubble is overestimated by these two turbulence models. On the contrary, at these locations, SBES overestimates the turbulent kinetic energy level. As a consequence, the recirculation bubble is shorter compared to experiments.

The Fig. 4 shows mean vertical velocity profiles at the location $x/L = -0.5$ in symmetry plane $Y/L = 0$ (left figure) and plane $Y/L = 0.5$ (right figure). As DDES shows the closest reattachment point on the rear slant surface compared to experiments in symmetry plane, the vertical velocity profil matchs perfectly with experiments. Moreover, this result shows that the thickness of the closed recirculation bubble from DDES model is the same compared to experimental results. Because of the quick reattachment given by SBES model, the vertical velocity is low compared to experiments as the flow has a downwash move earlier. The same conclusion can be drawn for SAS model as the bubble is over-estimated.
For the plane $Y/L = 0.5$, all the velocity profiles show some discrepancies regarding experiments. The higher velocity for DDES clearly indicates that the recirculation

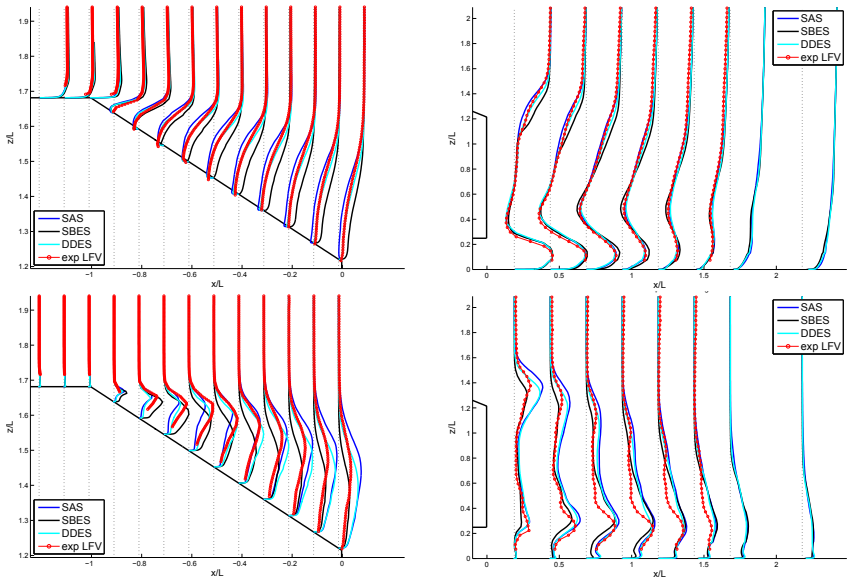

Fig. 3 Comparisons of mean streamwise velocity $\overline{U_x}$ (top) and mean total turbulent kinetic energy $\overline{TKE}$ (bottom) between experiments (red), SAS (blue), SBES (black) and DDES (cyan) − zoom on the rear slant surface (left) and on the wake of the body (right) symmetry plane $Y/L = 0$

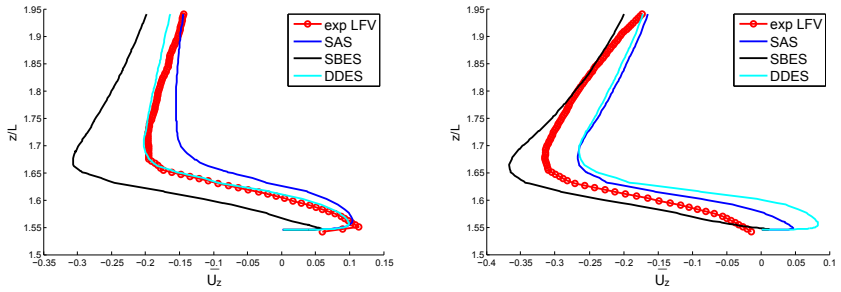

Fig. 4 Comparisons of mean vertical velocity $\overline{U_z}$ between experiments (red), SAS (blue), SBES (black) and DDES (cyan) − zoom on the rear slant surface in symmetry plane $Y/L = 0$ (left) and plane $Y/L = 0.5$ (right)

bubble thickness is slightly over estimated, as with SAS model. On the contrary, the SBES model still under-estimates the bubble thickness because of short closed recirculation on the rear surface.

7 Conclusions

A Scale Resolving Simulation strategy has been used to study the flow around a 25°Ahmed body. The results obtained for the Reference grid shown are encouraging for future works on real car. DDES shows the best prediction of the flow compared to experiments. The length of the closed recirculation bubble on the rear slant angle is equal to 90% compared to 78% in experiments. Drag coefficient is very well estimated and lift coefficient suffers with a 6% error compared to experiments. Moreover, mean velocity and TKE profiles attest the superiority of DDES to SAS and SBES on this grid. However, the grid convergence study shows the strong influence of the mesh on DDES capability to correctly predict the flow around the body. SAS and SBES, based on their formulations, are more robust to grid modifications.

References

1. Ahmed, S. R., G. Ramm, G. Faltin: Some salient features of the time-averaged ground vehicle wake. No. 840300. SAE Technical Paper (1984)
2. ANSYS Fluent Theory Guide, Release 17.0 (2016)
3. Ashton, N., A. Revell: Key factors in the use of DDES for the flow around a simplified car. International Journal of Heat and Fluid Flow **54**, 236–249 (2015)
4. Guilmineau, E.: Computational study of flow around a simplified car body. Journal of wind engineering and industrial aerodynamics, **96(6)**, 1207–1217 (2008)
5. Guilmineau, E., Deng, G., Wackers, J.: Numerical simulation with a DES approach for automotive flows. Journal of Fluids and Structures, **27(5)**, 807–816 (2011)
6. Haase, W., Aupoix, B., Bunge, U., Schwamborn, D. (Eds.).: FLOMANIA-a European initiative on flow physics modelling: results of the European-Union funded project, 2002-2004 Vol. 94 Springer Science & Business Media (2006)
7. Kapadia, S., Roy, S., Vallero, M., Wurtzler, K., Forsythe, J.: Detached-eddy simulation over a reference Ahmed car model. In Direct and Large-Eddy Simulation V. Springer Netherlands, 481–488 (2004)
8. Krajnović, S., Davidson, L.: Flow around a simplified car, part 1: large eddy simulation. Journal of Fluids Engineering, **127(5)**, 907–918 (2005)
9. Menter, F. R., Zonal two equation k-ε turbulence models for aerodynamic flows. AIAA paper, 2906 (1993)
10. Menter, F. R., Kuntz, M.: Adaptation of eddy-viscosity turbulence models to unsteady separated flow behind vehicles. In The aerodynamics of heavy vehicles: trucks, buses, and trains. Springer Berlin Heidelberg, 339–352 (2004)
11. Menter, F. R., Egorov, Y.: The scale-adaptive simulation method for unsteady turbulent flow predictions. Part 1: theory and model description. Flow, Turbulence and Combustion, **85(1)**, 113–138 (2010)
12. Minguez, M., Pasquetti, R., Serre, E.: High-order large-eddy simulation of flow over the Ahmed body car model. Physics of Fluids (1994-present), **20(9)**, 095101 (2008)
13. Rossitto, G., Sicot, C., Ferrand, V., Bore, J., Harambat, F.: Influence of afterbody rounding on the pressure distribution over a fastback vehicle. Experiments in Fluids, **57(3)**, 1–12 (2016)
14. Spalart, P. R., Jou, W. H., Strelets, M., Allmaras, S. R.: Comments on the feasibility of LES for wings, and on a hybrid RANS/LES approach. Advances in DNS/LES, **1**, 4–8 (1997)
15. Spalart, P.R., Deck, S., Shur, M., Squires, K.D., Strelets, M., Travin, A.: A new version of detached-eddy simulation, resistant to ambiguous grid densities, Theor. Comput. Fluid Dyn. **20**, 181–195 (2006)